HISTORY EFFECTS AND WALL SIMILARITY OF NON-EQUILIBRIUM TURBULENT BOUNDARY LAYERS IN VARYING PRESSURE GRADIENT OVER ROUGH AND SMOOTH SURFACES

Vidya Vishwanathan, Daniel J. Fritsch, K. Todd Lowe, William J. Devenport
Kevin T. Crofton Department of Aerospace
Ocean Engineering
Virginia Tech
Blacksburg, VA 24060
vidya418@vt.edu, dannyf96@vt.edu, kelowe@vt.edu, devenport@vt.edu

ABSTRACT

The effect of non-equilibrium pressure gradients and roughness on the behavior of turbulent boundary layers are investigated. In this experimental study, a family of systematically varying non-equilibrium pressure gradients was generated from the pressure field of a NACA 0012 airfoil over both smooth and rough wall surfaces. The rough surface consisted of 2 mm tall, staggered, circular cylindrical elements producing flow conditions that were in the fully rough regime. The behaviors of the velocity field were measured using a custom Pitot-probe rake and time-resolved particle image velocimetry (TR-PIV). The results show that the primary effect of the roughness is to increase the magnitude of the outer layer parameters. History effects, due to the changing pressure gradients, are apparent in the integrated boundary layer parameters indicating that rough and smooth wall flows are affected by both local and historical flow conditions. It is shown that indirect skin friction methods are sensitive to regression fits of the mean velocity profiles. Within the uncertainty of these empirical methods, the effective sandgrain roughness parameter appears to remain constant with streamwise and pressure gradient flow development, thus supporting the wall-similarity hypothesis for non-equilibrium rough wall flows.

INTRODUCTION

Turbulent boundary layers are omnipresent in a wide range of practical applications, such as over an aircraft wing or marine vehicle body. A wide range of studies have established a fundamental understanding of uni-directional pressure gradient flows (e.g., De Graaff & Eaton (2000); Joshi *et al.* (2014)). However, aside from use in controlled laboratory environments, these simple flows are just the building blocks for flows of practical interest. Real flows are susceptible to complex conditions impacted by both roughness and bi-directional pressure gradients (i.e., pressure gradients that switch sign). Surfaces in engineering application are usually not considered to be hydrodynamically smooth either due to macroscopic defects in the surface finish or due to naturally occurring roughness such as dirt, ice, or biofouling. Roughness can contribute to drag, unwanted vibrations, and noise, which can negatively impact the operation and design of vehicles. However, these flows are more difficult to model; thus improving the current array of knowledge for flows in non-equilibrium conditions is a relevant field of interest.

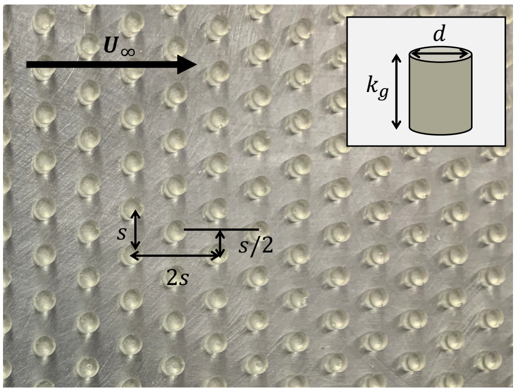

Figure 1. Staggered, circular cylindrical roughness configuration used in this study; $s = 6.93mm$, $d = 3.14mm$, $k_g = 2mm$. Inset shows features of a cylindrical element.

To understand the concept and behaviors of flows in non-equilibrium, it is useful to first establish what is considered to be a flow *in* equilibrium. Equilibrium conditions are idealized states in which flow properties are only dependent on local flow conditions, and the evolution of mean velocity and turbulence quantities with streamwise position can be collapsed by scaling on the basis of self-similarity (Devenport & Lowe (2022)). In a non-equilibrium turbulent flow, the local flow conditions are now also dependent on the history of conditions that the flow has experienced. In studies of smooth wall turbulent boundary layers induced by pressure gradients of changing signs, Fritsch *et al.* (2020) and Vishwanathan *et al.* (2021) have shown the impact of history effects on the fluctuating pressure and velocity features downstream of the pressure gradient switches. These are evidenced by a streamwise delayed response of the integrated boundary layer parameters and mean turbulence statistics with respect to the location of the pressure gradient switch.

For non-equilibrium rough wall flows a key question is the validity of the wall-similarity hypothesis, a concept first introduced by Townsend (1980), which suggests that on certain velocity parameter scalings, the boundary layer regions, outside of the immediate roughness vicinity, collapse to the equivalent conditions in a smooth wall flow. (Jiménez (2004)) refined the criteria for wall-similarity to specify roughness height (k_g) limitations with respect to either the effective sandgrain roughness (k_s) or the boundary layer thickness (δ). A number of studies (i.e., Raupach *et al.* (1991); Flack *et al.* (2005); Perry & Joubert (1963); Schultz & Flack (2005))have shown that for roughness sizes less than a certain factor of the boundary layer thickness (the exact factor varies between authors, but is typically taken as $\delta/k_s \geq 40$) roughness effects remain contained within the vicinity of the roughness sublayer, thus satisfying the question of wall-similarity. But enough studies, such as that by Aubertine & Eaton (2005), suggest that the current criteria for wall similarity is insufficient, and additional parameters relating to the pressure gradient conditions are necessary. As a majority of these studies have been conducted in equilibrium flow conditions, an evaluation of the wall-similarity hypothesis in non-equilibrium rough wall flows is needed.

The present work aims to understand the behavior of high Reynolds number wall-bounded turbulence induced under a systematically varying family of pressure gradients and discuss its compounding effects with roughness. In particular, investigations of the wall-similarity hypothesis of non-equilibrium rough wall flows are made and traditional analytical methods to determine roughness parameters are scrutinized. This experimental work largely uses the results from mean and instantaneous velocity fields measured using time-resolved particle image velocimetry (TR-PIV), a custom boundary layer rake, and other measures of mean flow conditions.

EXPERIMENTAL FACILITY

All measurements discussed in this paper were conducted in the Virginia Tech Stability Wind Tunnel (VT SWT), which is a closed-circuit facility. The empty tunnel freestream turbulence levels vary between 0.01% and 0.023% depending on the flow speed, owing to seven turbulence reducing screens in the settling chamber. The test section extends 7.32 m and has a square cross section 1.85 m on edge. The test section side walls consist of 0.61 m length modular square aluminum panels that are carefully levelled to produce a continuous boundary layer flow surface. The boundary layer is tripped 3.58 m upstream of the test section entrance and by the first measurement plane, is close to 51 mm thick in smooth wall and 62 mm thick in rough wall configurations. These panels are arranged in a grid pattern that can be removed and replaced with panels with custom instrumentation and wall conditions. The data discussed in this paper were measured at a Reynolds number per meter of 2.18 million based on the inflow freestream velocity, which at the time of the rough and smooth wall experimental studies was between $U_\infty = 33 - 36$ m/s.

ROUGHNESS GEOMETRY

A portion of the rough surface used in this study is shown in Figure 1. The surface entails a staggered pattern array of circular cylindrical elements that have a roughness height of $k_g = 2$ mm and diameter of 3.14 mm and are periodic on a 0.61 m x 0.61 m pattern (corresponding to the size of the removable test section panels). As shown in the test schematic in Figure 2, the rough wall starts at the test section entrance and extends 5.43 m downstream covering the entire port side test section wall. The elements are spaced $s = 6.93$ mm apart in the streamwise direction, and half this distance in the spanwise direction. The roughness elements were fabricated from epoxy using HDPE molds that were CNC milled with insets in the element shape. The mold was then overlaid on an aluminum test section panel and vacuum bag sealed for 24 hours of cure time. For ease of fabrication, the cylindrical element tips were tapered by 1^o. Given current skin friction estimates computed from regression fits of the rough wall law of the wall, the roughness Reynolds number ranges between $k_s^+ = 243 - 488$. Thus, this flow is in the fully rough regime.

MECHANISM FOR WALL PRESSURE GRADIENT

A 0.914 m chord NACA 0012 airfoil, swept to both positive and negative angles of attack, generated a systematically varying family of closely two-dimensional pressure gradients on the test section walls. The airfoil quarter chord was positioned at $x = 3.45$ m and $y = 0.925$ m with respect to the coordinate origin. Figure 2 shows a top-down schematic, of the test section configuration. The magnitude of the pressure gradient was computed using the Clauser pressure gradient parameter defined as $\beta = (\partial p/\partial x)\delta^*/\tau_w$, where δ^* is the displacement thickness. In this experiment the pressure gradients were mild (i.e. no relaminarization nor separation), and ranged between $-0.8 < \beta < +0.78$. Because of the nominally symmetric airfoil and test section, both of the side walls experience the same flow families. However, for ease of measurement access, the boundary layer wall of interest considered in this study was the "port" side wall corresponding to the lower wall in Figure 2. The boundary layer wall experiences both an adverse and favorable pressure gradient. It should be noted that this is not an airfoil experiment; the airfoil is simply used as a mechanism to induce the pressure gradients.

Figure 3 shows the distribution of β, on the instrumented portion of the center streamline on the boundary layer wall of interest. A comparison of the rough and smooth wall pressure gradient distributions is shown in solid and dashed lines, respectively. At positive angles of attack the boundary layer wall experiences an APG which switches to a FPG at a streamwise location approximately adjacent to the airfoil quarter-chord. The opposite phenomena are experienced by the wall when the airfoil is at negative angles of attack. The β distributions show a systematic set of pressure gradients. Upstream of $x = 3.45$ m these vary from mildly favorable at negative angle of attack to mildly positive at positive angle of attack, and are very similar for the smooth wall and rough wall boundary layers. Downstream of this station, the pressure gradients switch sign and the rough and smooth wall flows start to show markedly different behavior, with significantly greater positive beta excursions for the rough wall.

MEASUREMENT SYSTEMS

The two sidewalls of the test section were equipped with 82 static pressure taps each. The taps were carefully flush mounted to the inner wall/roughness substrate and had a 0.1 mm inner diameter. The mean surface pressure distributions were measured using an Esterline 9816/98RK pressure scanner with a range of ± 10" H_2O and a 32-channel DTC Initium scanner with a range of ± 4" H_2O. The reference pressure was measured as the ambient pressure in the control room.

A custom 30-Pitot probe boundary layer rake was used to measure the mean velocity profiles at the streamwise locations indicated by the black stations labeled on Figure 2. The probes extend 178 mm from the wall, a sufficient length for capturing the full rough and smooth wall boundary layer thicknesses. The probe ports were connected to a 20" H_2O pressure range DTC ESP 32HD pressure scanner. Bernoulli's equation for stagnation pressure was used to extract the velocity boundary

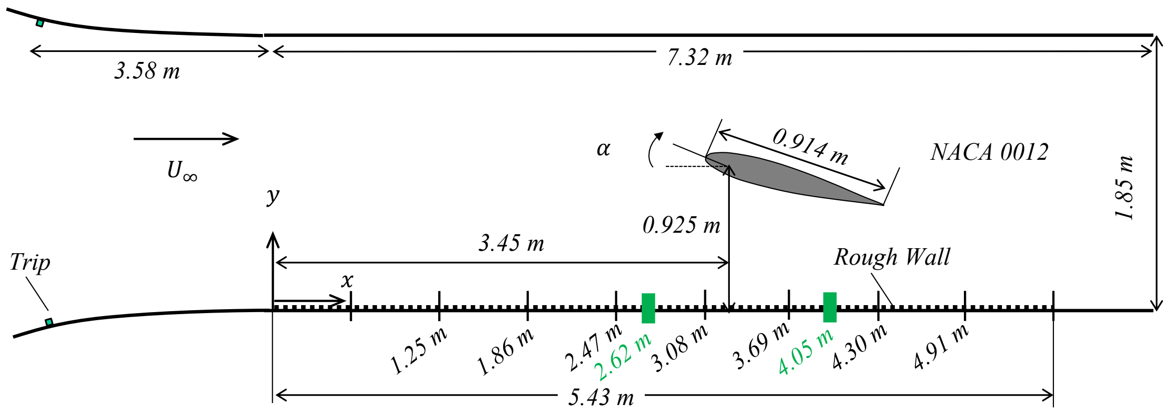

Figure 2. Top-down schematic of the test section. Boundary layer wall of interest is the "port" wall, seen here as the lower wall, which was either in smooth or rough wall configuration. Measurement locations of the boundary layer rake and TR-PIV are indicated in vertical black and green lines, respectively.

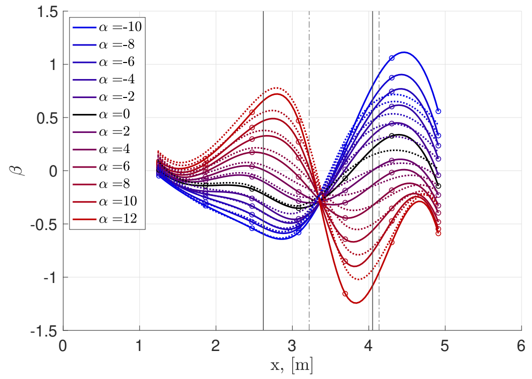

Figure 3. Streamwise variation of the Clauser pressure gradient parameter, β, as a function of the NACA 0012 angle of attack shown at the boundary layer rake measurement locations. Solid lines are the rough wall, dashed lines are the smooth wall. Vertical dashed lines indicate locations of the airfoil leading and trailing edge, respectively. Vertical solid lines indicate the locations of the TR-PIV measurements. Color legend is used for subsequent figures unless otherwise noted.

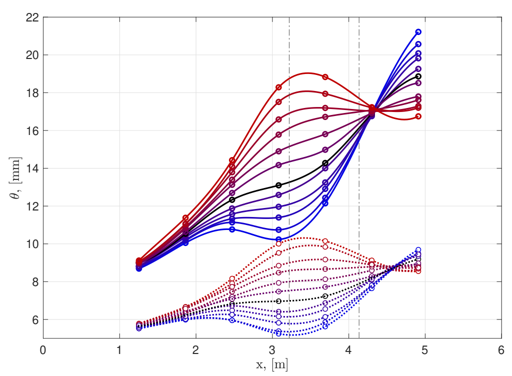

Figure 4. Momentum thickness variation with streamwise distance and NACA 0012 angle of attack. Solid line is rough wall, dashed line is smooth wall.

layer profile from the wall. All mean velocity profiles and integrated boundary layer parameters discussed in this paper were measured using the boundary layer rake.

Time-resolved PIV measurements were made at two streamwise planes corresponding to the upstream and downstream locations of maximum pressure gradient, occurring approximately at $x = 2.62$ m and $x = 4.05$ m. The TR-PIV measurement locations are labeled in green in Figure 2 and indicated by the vertical solid lines in Figure 3. The smooth wall measurements were made in planar 2D, two component configuration in which 10,000 realizations were recorded in double-frame mode at a sampling rate of 12.5 kHz. The rough wall measurements were made in a stereoscopic 2D three-component configuration, in which 24,839 time realizations were recorded at a 1 kHz sampling rate. Further information regarding the specifics of the PIV hardware system can be found in Vishwanathan *et al.* (2021). The camera and lens configurations resulted in spatial resolutions of 2.50 mm for the smooth wall and 2.25 mm for the rough wall. The conversion from raw image to velocity field was completed in LaVision's DaVis10 and then the data were post-processed for statistics in MATLAB. All turbulence stress profiles discussed in this paper were measured using the TR-PIV system.

BOUNDARY LAYER DEVELOPMENT

Figure 4 shows the streamwise and pressure gradient dependent progression of the momentum thickness θ for the rough and the smooth wall. As expected, the effect of the roughness is to increase the magnitudes of the integrated boundary layer parameters. Although a similar functional trend of pressure gradient response is seen in both the smooth and rough wall flows, the slope of the curves appears to be steeper for the rough wall, indicating that in addition to the absolute thicknesses, the rate of the boundary layer growth is increased due to the pressure drag from the roughness elements. At positive angles of attack, the naturally occurring flat plate boundary layer thickness is exacerbated due to the presence of the initial APG flow. This is followed by a decrease in growth rate after the flow has transitioned to the FPG downstream of the airfoil quarter chord. At negative angles of attack, the flow is initially accelerated due to the FPG. This is followed by flow deceleration and an increase in the boundary layer growth rate due to the transition to APG. The integrated boundary layer parameters for the rough wall also show a crossover downstream

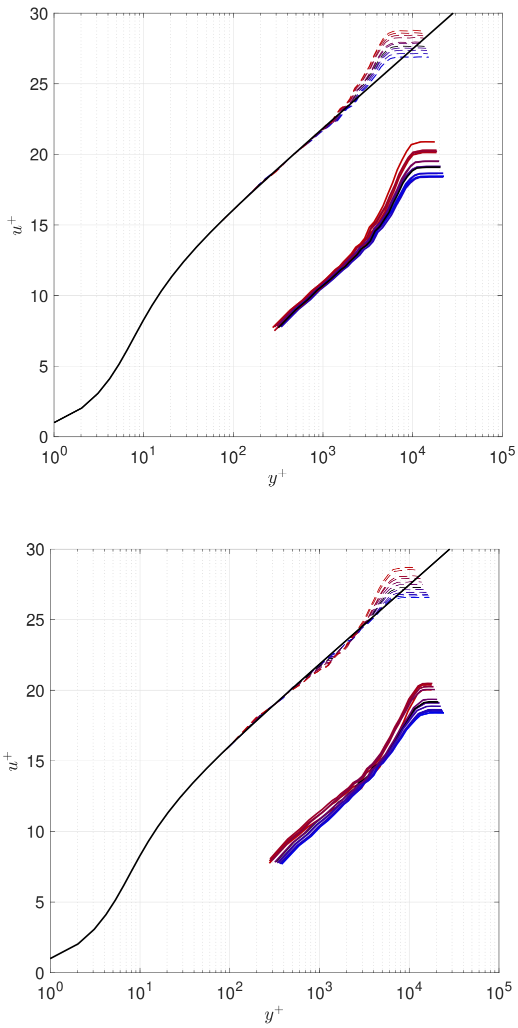

Figure 5. Mean velocity profiles normalized on inner coordinates for rough (solid colored lines) and smooth (dashed lines) configurations at (top) $x = 2.62$ m and (bottom) $x = 4.05$ m. Solid black line is the Spalding curve (Spalding (1961).)

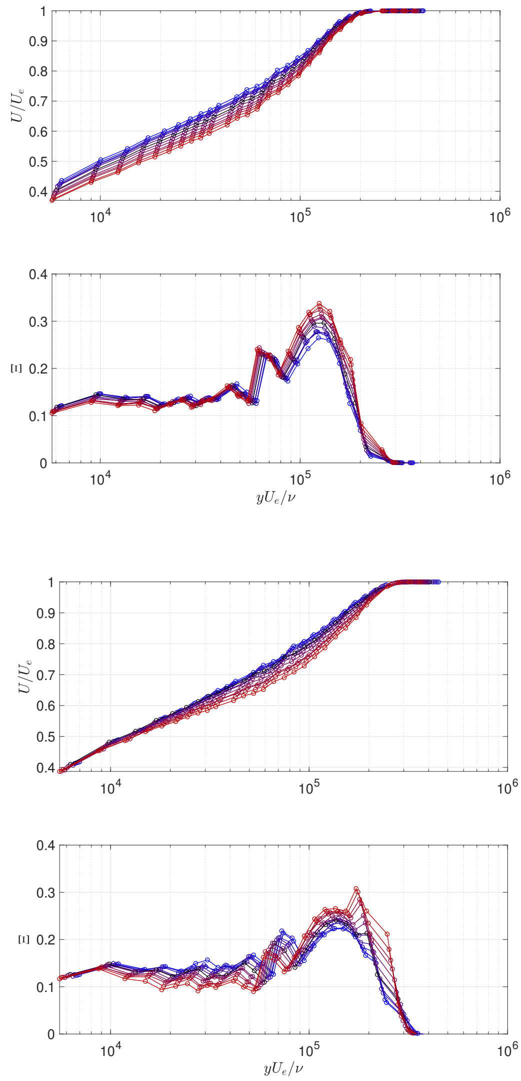

Figure 6. Logarithmic-law diagnostic function used to select the logarithmic region for regression fit methods to determine skin friction from mean velocity profiles; (top) $x = 2.62$ m and (bottom) $x = 4.05$ m.

of the pressure gradient transition, a behavior already observed in previous studies of the smooth wall by Fritsch *et al.* (2020) and Vishwanathan *et al.* (2021), a behavior that is attributed to a delayed response to the upstream flow history.

MEAN VELOCITY PROFILES

Figure 5 shows mean velocity profiles for both the rough wall and smooth wall at x = 2.62 m (before the pressure gradient sign change) and at x = 4.05 m (after the pressure gradient sign change). The varying pressure gradient magnitudes cause the wake strength to increase with progressive streamwise locations. The effect of the roughness is to increase the shear velocity, thus causing a downward shift of the mean velocity profiles, which appears as the extra term, ΔU^+ in the law of the wall for rough wall flows. The rough wall mean velocity profiles in Figure 6 are normalized on outer coordinates. Under this normalization, the mean velocity deficit due to the impacts of the initially APG (red curves) become apparent, especially at the $x = 4.05$ m station (see bottom set of mean velocity profiles in Figure 6). At this condition, the mean velocity gradient is decreased, and the logarithmic region develops a dip in the profile shape, a deficit that is larger when the upstream APG magnitude is higher. The slope of the logarithmic region is decreased which introduces sensitivities to the mean velocity regression fits used to indirectly determine skin friction. Although not shown here, Vishwanathan *et al.* (2021), saw similar velocity deficit trends in the smooth wall mean velocity profiles as well.

REYNOLDS STRESS PROFILES

Streamwise Reynolds normal stresses for locations before and after the pressure gradient switch (i.e. $x = 2.62$ m and $x = 4.05$ m, respectively) are shown for both the rough and smooth wall in Figure 7. Conditions at the most adverse, favorable, and nominally zero pressure gradient conditions are plotted ($\alpha = +12^o, 10^o, 0^o$, respectively). Due to limitations of the TR-PIV camera field of view with respect to the boundary layer thickness at $x = 4.05$ m, the full wall-normal turbulence stress profile was not captured. At $x = 2.62$ m, the turbulence

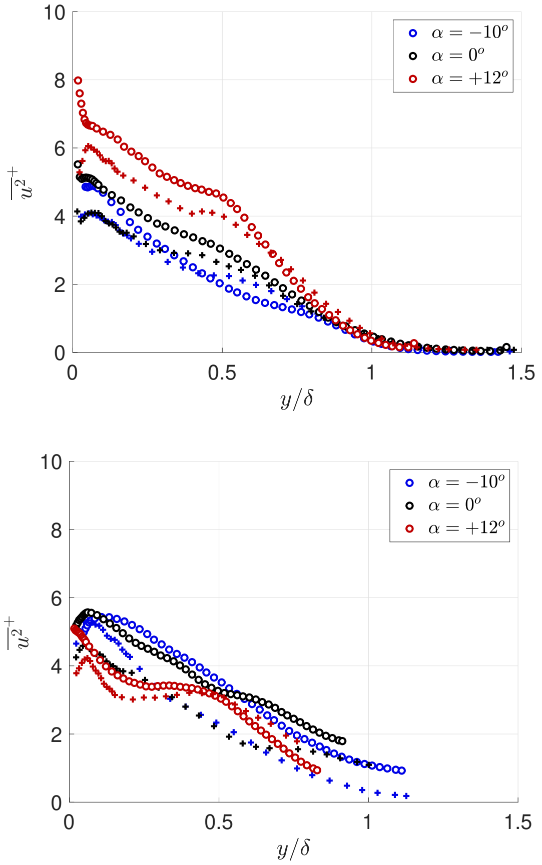

Figure 7. Reynolds streamwise normal turbulence stress plotted on inner-outer coordinates for the rough (○) and smooth wall (+); (top) $x = 2.62$ m and (bottom) $x = 4.05$ m.

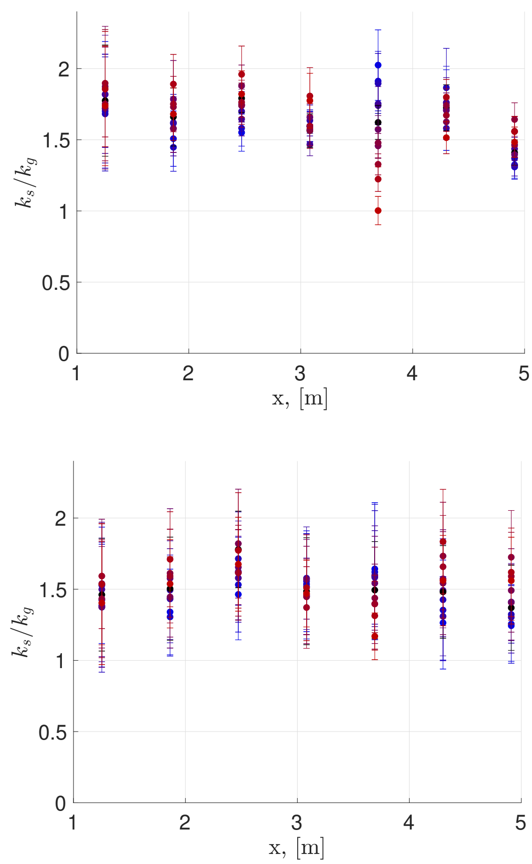

Figure 8. Effective sandgrain roughness parameter (k_s) normalized by roughness height (k_g) computed from a regression fit of the mean velocity profiles. (Top) the selected logarithmic region is custom to each flow condition, and (bottom) the logarithmic region is taken to be between $8680 < yU_e/\nu < 21270$.

stress magnitudes for the initially APG flow are higher than when the flow is initially in the FPG. This trend reverses after the pressure gradient sign switch as the flow approaches the station at $x = 4.05$ m. In both the rough and smooth wall flows, the Reynolds normal stress is increased as the flow switches from a FPG to an APG (blue curves), and decreased as the flow switches from an APG to a FPG (red curves). However, a secondary peak becomes more prominent in the red profiles at $x = 4.05$ m. It appears that the near-wall turbulence production, which was instigated at the earlier streamwise station, is diffused away from the wall as the flow approaches the station at $x = 4.05$ m, resulting in the intensified second peak. This response to the pressure gradient is observed in both the rough and smooth wall Reynolds streamwise normal stresses. Outer-layer similarity appears to be demonstrated in the flow plane at $x = 2.62$ m evidenced by a collapse of the smooth and rough wall turbulence stress profiles in the region outside of the roughness sublayer. It is hypothesized that the wall-similarity actually extends further into the boundary layer, but is obscured by an under measurement of the stresses due to the relatively coarse spatial resolution of the TR-PIV cameras.

WALL-SIMILARITY OF THE ROUGH WALL FLOW

As direct measurements of wall shear stress are not always feasible, particularly with rough wall flows, empirical methods, such as mean velocity profiles fits and momentum integral analyses to determine skin friction from velocity field data have often been used in the literature instead. It is commonly agreed that these methods inherently have their flaws and result in high uncertainty for the computed shear velocities, u_τ (Aubertine *et al.* (2004)). However, in the absence of direct measurements and with the acknowledgement of these uncertainties, these methods can still provide an estimate of the shear stress in the flow. Their validity in a non-equilibrium flow environment is yet to be thoroughly evaluated. In the present study the regression fit method by Perry & Joubert (1963) is used to estimate skin friction from the mean velocity profiles. In this method, the law of the wall for rough walls is rearranged in terms of the velocity normalized on the boundary layer edge velocity, U_e, such that the slope and intercept of the curve are functions of the skin friction and roughness parameter, ΔU^+. Then, the effective sandgrain roughness is computed from the following relation:

$$\Delta U^+ = \frac{1}{\kappa} ln(k_s^+) - 3.5$$

Where κ is the von Kármán constant and is taken to be 0.41.

Like many mean velocity fit methods, the resulting skin friction depends on the selection of the logarithmic region, which relies upon on engineering judgement. In an attempt to provide quantitative feedback on the selected region used for the regression fits, the logarithmic law (log-law) diagnostic function, introduced for the smooth wall by Österlund *et al.*

(2000), was used. Due to the independence of the roughness function parameters from wall-normal position, the rough wall form of log-law diagnostic function remains the same as that of the smooth wall:

$$\Xi = \left(\frac{yU_\infty}{\nu}\right) \frac{d(U/U_\infty)}{d(yU_\infty/\nu)}$$

Figure 6 shows the log-law diagnostic function for flow conditions before and after the pressure gradient switch. The logarithmic region is considered to be within the region of constant Ξ, and provides the basis for selecting the points used in the mean velocity regression fits. By varying the number of logarithmic points, it was shown that the resulting skin friction, and by extension the roughness parameter, was sensitive to the selection of the logarithmic region. In this analysis, the number of points in the regression fit was varied and a corresponding k_s was recomputed. The number of permutations for points considered was limited to only include points taken from the near-wall to the furthest point with constant Ξ. A 95% confidence interval using a Student's t-distribution is plotted as the error bars on Figure 8. This figure shows a variation of the normalized k_s on the roughness height k_g depending on the selected logarithmic region. The location that appears to have a higher sensitivity to this log-region selection is the location immediately after the flow has switched from APG to FPG, which can be attributed to the more pronounced mean velocity deficit that reduces its logarithmic shape. However, despite a lower than expected estimate of the uncertainty, there is no discernible functional dependence of the local or historical effects on the normalized sandgrain roughness parameter. This suggests that the effect of the roughness is contained within the roughness sublayer and that the non-equilibrium flow features do not impact the roughness function. Thus, within the uncertainty of the empirical method used to determine the skin friction, the k_s/k_g ratio appears to remain constant with pressure gradient, and the wall-similarity hypothesis for non-equilibrium rough wall flows is supported.

CONCLUSIONS

An experimental study of non-equilibrium turbulent boundary layers over rough and smooth surfaces was conducted in the Virginia Tech Stability Wind Tunnel. A NACA 0012 airfoil was used as a mechanism to induce a systematically varying family of pressure gradients on the boundary layer walls. Mean and instantaneous measurements of the velocity field were made using a boundary layer rake and time-resolved particle image velocimetry. The trend of the momentum thickness variation with streamwise development and non-equilibrium pressure gradient is very similar between the rough and smooth wall flows. However, the effect of the roughness is to increase the boundary layer magnitude and growth rate. Streamwise normal turbulence stresses show an increase in the outer layer energy after the pressure gradient switch, presumably due to an outward diffusion of turbulence produced in the near-wall at an upstream station prior to the pressure gradient sign change. Indirect methods to determine skin friction, specifically using regression fits of the mean velocity profiles, show high sensitivity of the selected logarithmic region on the computed shear stresses. Despite the inherent uncertainties of such methods, the wall-similarity hypothesis appears to be valid in a rough-wall non-equilibrium flow.

ACKNOWLEDGEMENTS

The authors would like to thank the Office of Naval Research, Dr. Peter Chang, and Dr. Julie Young for support under grants N00014-19-1-2109, N00014-18-1-2455, and N0014-20-1-2821. The authors are also grateful to VT Stability Wind Tunnel research staff and faculty, AOE Machine Shop, and fellow research students for their support and assistance in the experimental preparation and testing.

REFERENCES

Aubertine, Carolyn D & Eaton, John K 2005 Turbulence development in a non-equilibrium turbulent boundary layer with mild adverse pressure gradient. *Journal of Fluid Mechanics* **532**, 345–364.

Aubertine, Carolyn D., Eaton, John K. & Song, Simon 2004 Parameters controlling roughness effects in a separating boundary layer. *International Journal of Heat and Fluid Flow* **25** (3), 444–450.

De Graaff, David B. & Eaton, John K. 2000 Reynolds-number scaling of the flat-plate turbulent boundary layer. *Journal of Fluid Mechanics* **422**, 319–346.

Devenport, William J & Lowe, K Todd 2022 Equilibrium and non-equilibrium turbulent boundary layers. *Progress in Aerospace Sciences* **131**, 100807.

Flack, Karen A., Schultz, Michael P. & Shapiro, Thomas A. 2005 Experimental support for townsend's reynolds number similarity hypothesis on rough walls. *Physics of Fluids* **17** (3), 035102.

Fritsch, Danny, Vishwanathan, Vidya, Duetsch-Patel, Julie, Gargiulo, Aldo, Lowe, Kevin T & Devenport, William J 2020 The pressure signature of high reynolds number smooth wall turbulent boundary layers in pressure gradient family. In *AIAA Aviation 2020 Forum*, p. 3066.

Jiménez, Javier 2004 Turbulent flows over rough walls. *Annual Review of Fluid Mechanics* **36** (1), 173–196.

Joshi, Pranav, Liu, Xiaofeng & Katz, Joseph 2014 Effects of fluctuating pressure gradients on boundary layer turbulence. *Journal of Fluid Mechanics* **748**, 36.

Perry, A. E. & Joubert, P. N. 1963 Rough-wall boundary layers in adverse pressure gradients. *Journal of Fluid Mechanics* **17** (2), 193–211.

Raupach, M. R., Antonia, R. A. & Rajagopalan, S. 1991 Rough-wall turbulent boundary layers. *Applied Mechanics Reviews* **44** (1), 1–25.

Schultz, M. P. & Flack, K. A. 2005 Outer layer similarity in fully rough turbulent boundary layers. *Experiments in Fluids* **38** (3), 328–340.

Spalding, DB 1961 A single formula for the law of the wall. *Journal of Applied Mechanics* **28** (3), 455–458.

Townsend, AAR 1980 *The structure of turbulent shear flow*. Cambridge university press.

Vishwanathan, Vidya, Fritsch, Danny, Lowe, Todd K & Devenport, William J 2021 Analysis of coherent structures over a smooth wall turbulent boundary layer in pressure gradient using spectral proper orthogonal decomposition. In *AIAA Aviation 2021 Forum*, p. 2893.

Österlund, Jens M., Johansson, Arne V., Nagib, Hassan M. & Hites, Michael H. 2000 A note on the overlap region in turbulent boundary layers. *Physics of Fluids* **12** (1), 1–4.